Formation of Au−Ag Core−Shell Nanostructures in Silica Matrix by Sequential Ion Implantation

Ovidio Peña,[†] Umapada Pal,*[,†] Luis Rodríguez-Fernández,[‡] Héctor G. Silva-Pereyra,[‡] Vladimir Rodríguez-Iglesias,[‡] Juan Carlos Cheang-Wong,[‡] Jesús Arenas-Alatorre,[‡] and Alicia Oliver[‡]

Instituto de Física, Benemérita Universidad Autónoma de Puebla, Apartado Postal J-48, Puebla, Puebla 72570, México, and Instituto de Física, Universidad Nacional Autónoma de México, Apartado Postal 20-364, México D.F. 01000, México

Received: October 16, 2008; Revised Manuscript Received: December 24, 2008

Formation of Au core−Ag shell bimetallic nanoparticles in silica matrix is demonstrated through sequential implantation of Ag and Au ions and subsequent thermal annealing. Formation of core−shell structures is verified through optical absorption spectroscopy, high-resolution transmission electron microscopy, electron energy loss spectroscopy, and simulated optical extinction spectra. A mechanism for the formation of such unusual structures in ion-implanted silica is proposed. By controlling the implantation energy of the two ions properly and keeping the implantation sequence Ag first and then Au, it is possible to create Au core−Ag shell nanoparticles in the silica matrix with homogeneous distribution.

Introduction

Nanometer-size particles have been the subject of increasing attention in recent years due to their unique properties and wide range of prospective applications. Metallic nanoparticles (NPs) embedded in glasses are particularly important because of their interesting optical properties with a high potential for applications in optical and optoelectronic devices.[1] Large third-order susceptibility and optical response times in picoseconds range make them excellent candidates for using in catalysis,[2] optoelectronics,[3−6] and magnetic information storage.[7] Among the techniques used to obtain these NPs, ion implantation stands for its several advantages: it allows the synthesis of materials which are not obtainable by conventional glass melting techniques and both the concentration of the implanted ions and their distribution as a function of depth can be controlled to a certain degree.

Along with the size and shape, the other parameter that strongly affects the optical properties of the NPs is the composition. By combining two different metals, it is possible to obtain three different kinds of arrangements: mixture of monometallic NPs, bimetallic alloy NPs, and core−shell structures (one material forms a solid core and the other a surrounding shell), all of which produce quite different optical responses. The first case is of little interest since it produces only a two-peak extinction spectrum that is the averaged sum of the extinction spectra of the NPs of constituent metals. On the other hand, core−shell and alloy structures are of great interest. In the core−shell structures, change in dielectric constant occurs at the core−shell boundary[1] and the shell can be used as a protective layer. For instance, a gold shell can be used to improve the chemical stability of silver-based surface plasmon resonance (SPR) devices.[8] The interest in the alloy-type NPs lies on the fact that by changing the relative composition of the metals, homogeneous changes are produced in the dielectric constant,[8,9] which can be used to tune the position as well as the width of the SPR peaks according to the requirements.

It is obvious that before the bimetallic NPs reach their full application potential, a careful control over their synthesis and stability has to be performed. Unfortunately, there are many factors involved in their formation, and therefore, it is often not possible to determine a priori which type of particles a given preparation method will create. Particularly, in the case of ion implantation, some other important factors like the miscibility of the implanted elements, their interaction with the host matrix, and the creation of radiation-induced defects, which can influence the nucleation and growth of the clusters,[1,9] are involved. In the case of Ag−Au composites created by ion implantation, despite of the fact that several groups have reported the formation of alloy-based structures,[8−11] to the best our knowledge, in none of the cases core−shell structures were obtained. Nevertheless, it should be noted that some theoretical studies[12−14] on the structure and chemical ordering of Ag−Au free nanoparticles show that Ag−Au nanoparticles should adopt either an intermixed structure (with some silver enrichment of the surface) or a Au core−Ag shell structure.

In the present work we studied the conditions that allow the formation of Au−Ag core−shell structures by sequential ion implantation of the two elements in the silica matrix and subsequent thermal annealing. The optical response and structural characteristics of the obtained NPs were analyzed by means of optical absorption spectroscopy (OAS), high-angle angular dark field (HAADF), electron energy loss spectroscopy (EELS), and high-resolution transmission electron microscopy (HRTEM). A comparison between the calculated and the experimental extinction spectra was used to determine the nature (core−shell or alloy-type structure) of the obtained NPs. As the HAADF image contrast is approximately proportional to $Z^{1.7}$,[15] the location of the elements in core−shell structures could be determined from them. Due to enough difference between the atomic numbers of Ag (47) and Au (79), the *Z*-contrast imaging

* Corresponding author. E-mail: upal@sirio.ifuap.buap.mx. Fax: +52-222-2295611.
[†] Benemérita Universidad Autónoma de Puebla.
[‡] Universidad Nacional Autónoma de México.

10.1021/jp809178y CCC: $40.75
Published on Web 01/22/2009

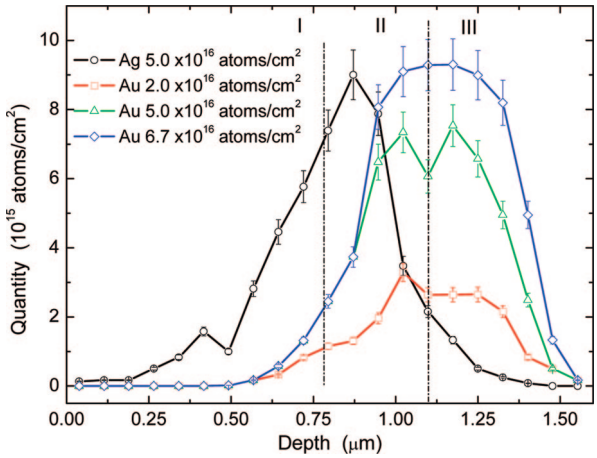

Figure 1. Depth profiles of Au and Ag distributions for the samples coimplanted with Ag (1.8 MeV) and Au (3.5 MeV) ions, obtained from the fitting of the corresponding RBS spectra.

could be used to determine the composition variations within the nanoparticles, and EELS is also able to recognize with great precision the location of each element. Additionally, HRTEM images of the nanoparticles were used to identify core−shell structure formation in them.

Experimental Section

High-purity silica glass plates (20 × 20 × 1 mm^3) with an OH content lower than 1 ppm, no individual impurity greater than 1 ppm, and a total impurity content less than 20 ppm were implanted at room temperature (RT) with a sequential implantation of 1.8 MeV Ag^+ ions at a fluence of 5.0 × 10^{16} ions/cm^2 and 3.7 MeV Au^+ ions at fluences of 2.0 × 10^{16}, 5.0 × 10^{16}, and 6.7 × 10^{16} ions/cm^2, using the 3 MV Tandem accelerator (NEC 9SDH2 Pelletron) of the Instituto de Física, UNAM. The as-implanted samples were cut into smaller pieces and annealed at 900 °C for 1 h in air, in order to produce the nucleation of the bimetallic nanoparticles.

The fluences of implantation and the depth profiles of ion distributions were determined by Rutherford backscattering spectrometry (RBS). The optical extinction spectra were obtained at RT using a Cary 500 double-beam spectrophotometer in the 300−800 nm wavelength range. The calculation of optical response of the core−shell structures was performed using the extension of the original Mie theory by Aden and Kerker.[16] For this purpose, the refractive indexes of bulk Au and Ag measured by Johnson and Christy[17] were used after introducing corrections due to the size of the NPs.[18] HAADF, EELS, and HRTEM analyses were performed in a JEOL-2010 FEG microscope with a point-to-point resolution of 0.19 nm and equipped with a GATAN imaging filter (GIF) and a GATAN digital micrograph system for image acquisition (version 3.7.0). For microscopic observations, a tripod polisher was used to generate cross-sectional samples. The final thicknesses of the samples were <100 nm, to be transparent to the electron beam. The lattice spacings were measured from the digital HRTEM micrographs through digital image analysis of reciprocal space parameters, according to the method proposed by de Ruijter et al.[19] This method allows the measurement of lattice spacing and lattice plane angles with 0.0001 nm and 0.1° precision, respectively.

Results and Discussion

Figure 1 shows the depth profile of Ag and Au distribution obtained from the fitting of the corresponding RBS spectra.

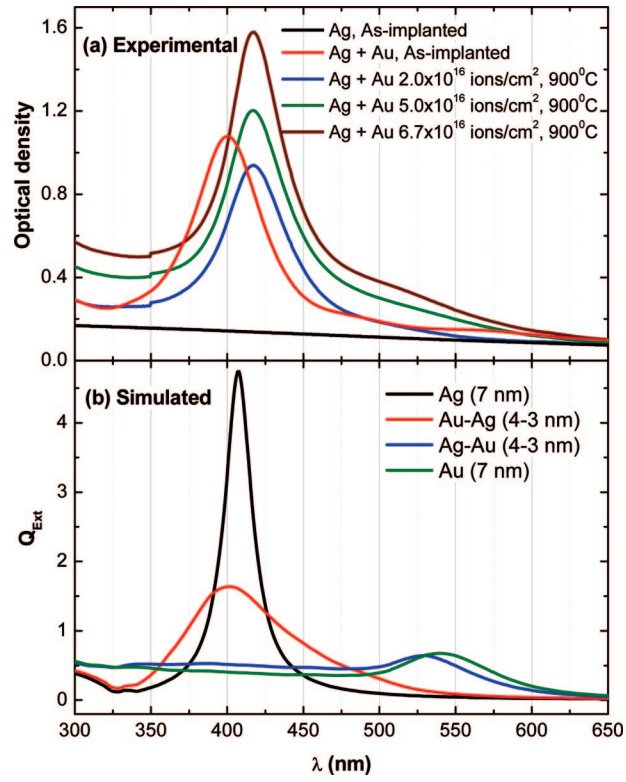

Figure 2. Experimental optical extinction spectra for the samples implanted with 5.0 × 10^{16} ions/cm^2 of Ag at 1.8 MeV and coimplanted with Au with different fluences at 3.5 MeV, before and after thermal annealing in air (a), and simulated extinction spectra for some possible configurations in silica matrix (b). Au−Ag means Au core−Ag shell, whereas Ag−Au means the opposite.

Although we chose the energies of the implanted species to obtain a maximum overlap (using previously calibrated data), the results show that during Au implantation Ag diffuses toward the sample surface. This effect creates three clearly defined zones in the depth profile of the final composite structure: zone I consisting mostly with Ag atoms, zone II with a mixture of Ag and Au atoms, and zone III consisting mostly with Au atoms. Therefore, we expected the formation of a certain amount of monometallic clusters in zones I and III and a considerable number of bimetallic NPs in zone II. As zone II was wide enough, formation and detection of bimetallic NPs in this region are expected.

Formation of Ag NPs in silica after the implantation of Au is clear in the experimental optical extinction spectra of the samples (Figure 2a). The SPR peaks for the coimplanted and annealed samples are similar to the one corresponding to the sample implanted only with Ag ions and annealed (not shown). However, the SPR peak position in the coimplanted samples exhibits small shifts (toward longer wavelength) with respect to the peak position of the Ag-only implanted sample, with no apparent regularity. The full width at half-maximum (fwhm) of the SPR peaks increases for all the coimplanted samples, and a small shoulder around 530 nm gets more noticeable with the increase of the Au fluence. From these results we can say that only a negligible amount of bimetallic alloy is actually formed, as otherwise it would produce noticeable shifts of the SPR peak, changing linearly its position from the Ag SPR position (400 nm) to the one corresponding to pure Au NPs (∼520 nm)[9] with the increase of Au fluence. As the observed small shifts are not attributable to the bimetallic structures, we consider that they are produced by the variations in refractive index of the matrix due to the implantation process.

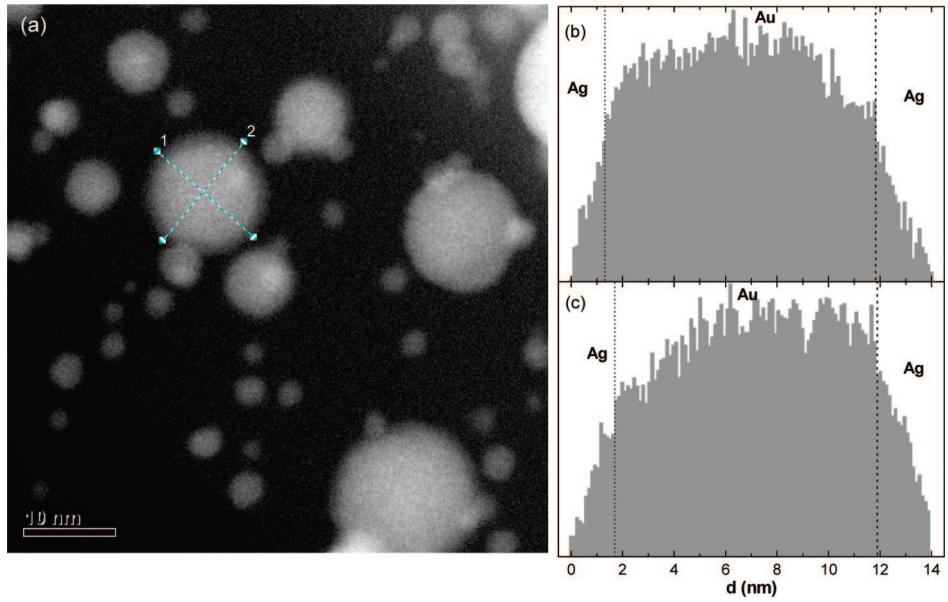

Figure 3. Typical HAADF micrograph of the sample coimplanted with 5.0×10^{16} ions/cm^2 of Ag at 1.8 MeV and 5.0×10^{16} ions/cm^2 of Au at 3.5 MeV after thermal annealing at 900 °C (a), and intensity profiles for the selected particle (b and c) showing the existence of core−shell structure.

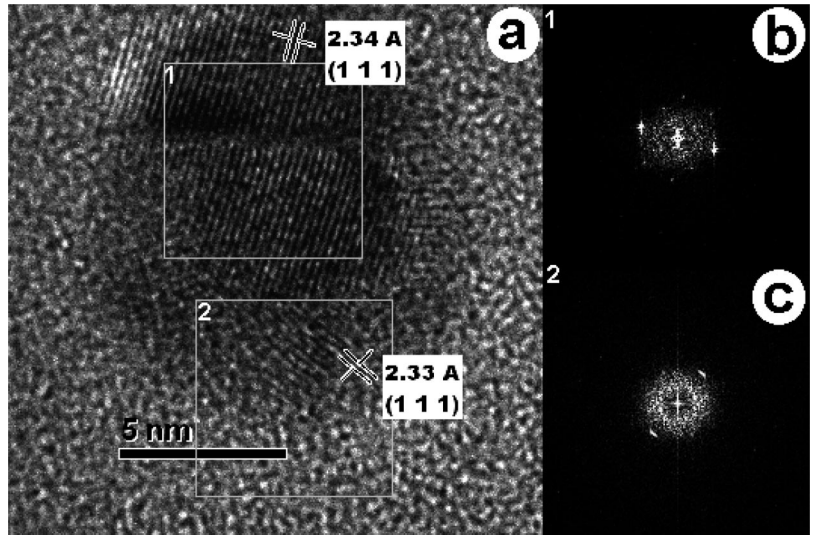

Figure 4. Typical HRTEM micrograph obtained for the sample coimplanted with 5.0×10^{16} ions/cm^2 of Ag at 1.8 MeV and 5.0×10^{16} ions/cm^2 of Au at 3.5 MeV after thermal annealing at 900 °C, showing a core−shell structure of around 12 nm of diameter (a), and the fast Fourier transform of the core (b) and the shell (c).

Since we expect to have a mixture of monometallic and bimetallic NPs in the samples (of unknown proportion), it is hard to compare directly the experimental results with simulations. Nevertheless, the calculations can be useful to provide a qualitative description of the effects involved. For instance, Figure 2b shows Mie simulations of the optical extinction spectra for core−shell configurations with different nanoparticle dimensions. As can be seen from the simulated spectra of Au core−Ag shell structures (red line), for this configuration the SPR peak widens and a shoulder band appears at around 500 nm, as seen in the experimental spectra. Therefore, it is possible that the widening of the SPR peak in the experimental spectra is caused by the presence of a given amount of core−shell structures, with Au core and Ag shell (because the inverse composition would produce a quite different optical extinction spectrum).

On the other hand, Figure 3a shows a HAADF micrograph obtained for the sample coimplanted with 5.0×10^{16} Au/cm^2. One can observe that monometallic as well as core−shell structures are present in the sample. From the intensity profiles of the images of selected nanoparticles (Figure 3, parts b and c), presence of Au at the core and Ag at the shell regions of the NPs can be confirmed. The presence of core−shell structures is also confirmed by the HRTEM images (Figure 4), apart from the OAS. Since the lattice parameters of Au and Ag are similar (4.078 Å for Au, JCPDS 4-0784; 4.077 Å for Ag, JCPDS 87-0720) are very close, it is impossible to differentiate them in the HRTEM image. However, the interplaner spacings obtained from them (Figure 4) confirm that both core and shell regions are oxide free.

Finally, in Figure 5a can be observed the superposition of two energy-filtering TEM images (Au−$O_{2,3}$ edge at 54 eV and Ag−$N_{2,3}$ edge at 56 eV). From there the presence of a gold core surrounded by a silver shell in some of the structures as well as a number of some monometallic gold NPs is clear. Additionally, an EELS analysis (Figure 5a) of the selected region

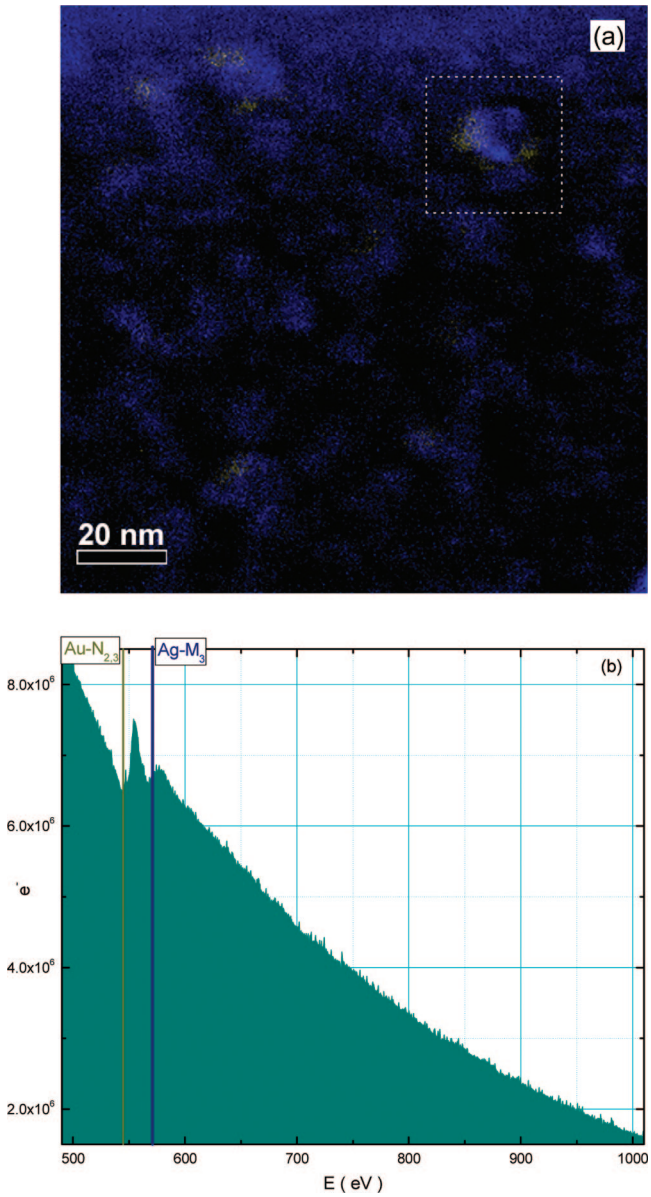

Figure 5. Core−shell structures obtained by the superposition of two energy-filtering TEM images (Au−$O_{2,3}$ edge at 54 eV and Ag−$N_{2,3}$ at 56 eV), showing gold in blue and silver in yellow (a) and the EELS analysis of the selected region for Au−$N_{2,3}$ edge at 545 eV and Ag M_3 edge at 571 eV (b).

further confirms the presence of Au and Ag at a different subshell energy (Au−$N_{2,3}$ edge at 545 eV and Ag M_3 edge at 571 eV).

Microscopic verification of the formation of core−shell configuration in supported nanostructures is really difficult. However, we have tried to visualize the presence of silver at the exterior of the Au−Ag bimetallic particles through HRTEM, HAADF, and energy-filtered TEM imaging techniques. In spite of the experimental difficulties, formation of Au core−Ag shell nanostructures in our samples has been demonstrated. To the best of our knowledge, this is the first report concerning the formation of such structures by coimplantation of Au and Ag ions in silica matrix. In contrast to our method, several research groups have implanted first the Au ions and the Ag ions later.[9,20] As Au has lower mobility in silica than Ag,[21,22] Au ions do not diffuse considerably during Ag implantation. Therefore, before the thermal annealing process, both Ag and Au remain dissolved in the matrix mainly in atomic form. It is probable that, on thermal annealing, these dissolved atoms form alloy NPs as observed in refs 9 and 20.

In our work, the ion implantation sequence was reversed, and because of silver's high motility, small Ag nanoparticles were formed even during the Au implantation, as indicated by the SPR peak at the position of the Ag plasmon before the thermal annealing. So, before thermal annealing there was a mixture of small Ag nanoparticles with Au atoms dissolved in the matrix. These conditions probably allowed the formation of small Au nanoparticles in the early stages of the thermal annealing. These Au nanoparticles act as nucleation centers, picking up neighboring Ag atoms or small Ag nanoparticles around them to form an outer shell of Ag through an Ostwald ripening mechanism. The presence of small Ag nanoparticles (of low HAADF contrast) around the core−shell structures (Figure 3a) also justifies the above-mentioned hypothesis.

Conclusions

In this work, we have demonstrated the formation of Au core−Ag shell bimetallic nanoparticles in silica matrix by sequential implantation of Ag and Au ions, followed by thermal annealing. Formation of core−shell nanoparticles was confirmed by OAS, HAADF, EELS, and HRTEM results. Sequential implantation of Ag and Au ions helps to form Ag NPs during the implantation of Au ions, and in as-prepared samples small Ag NPs remain in the silica matrix along with the dissolved Au atoms. On thermal annealing, dissolved Au atoms nucleate to form Au NPs, and the Ag NPs aggregate around them. The aggregated Ag NPs form a continuous shell around the Au particles through an Ostwald ripening process. Though in our study the core−shell NPs are formed only in region II, by controlling the implantation energy of the two ions properly and keeping the implantation sequence Ag first and then Au, it is possible to create Au core−Ag shell nanoparticles in the silica matrix with homogeneous distribution.

Acknowledgment. The authors thank K. López and F. J. Jaimes for the accelerator operation, J. G. Morales for his assistance in the annealing of the samples and L. Rendón for the TEM operation. This work was partially supported by CONACyT, México (Grant Nos. 46269 and 50504).

References and Notes

(1) Meldrum, A.; Boatner, L. A.; White, C. W. *Nucl. Instrum. Methods Phys. Res., Sect. B* **2001**, *178*, 7.
(2) Tihay, F.; Pourro, G. M.; Roger, A. C.; Kienneman, A. *Appl. Catal., A* **2000**, *206*, 24.
(3) Mazzoldi, P.; Arnold, G. W.; Battaglin, G.; Gonella, F.; Haglund, R. *J. Nonlinear Opt. Phys. Mater.* **1996**, *5*, 285.
(4) White, C. W.; Budai, J. D.; Withrow, S. P.; Zhu, J. G.; Souder, E.; Zuhr, R. A.; Meldrum, A.; Hembree, D. J.; Henderson, D. O.; Prawer, S. *Nucl. Instrum. Methods Phys. Res., Sect. B* **1998**, *228*, 141.
(5) Borsella, E.; Garcia, M. A.; Mattei, G.; Maurizio, C.; Mazzoldi, P.; Cattaruzza, E.; Gonella, F.; Battaglin, G.; Quaranta, A.; D'Acapito, F. *J. Appl. Phys.* **2001**, *90*, 5567.
(6) Pavesi, L.; Dal Negro, L.; Mazzoleni, C.; Franzo, G.; Priolo, F. *Nature* **2000**, *408*, 440.
(7) Chien, C. L. *Science and Technology of Nanostructures Magnetic Materials*; Plenum: New York, 1991; Vol. 259, p 477.
(8) Sharma, A. K.; Gupta, B. D. *Nanotechnology* **2006**, *17*, 124.
(9) Mattei, G. *Nucl. Instrum. Methods Phys. Res., Sect. B* **2002**, *191*, 323.
(10) Cattaruzza, E.; Battaglin, G.; Calvelli, P.; Gonella, F.; Mattei, G.; Maurizio, C.; Mazzoldi, P.; Padovani, S.; Polloni, R.; Sada, C.; Scremin, B. F.; D'Acapito, F. *Compos. Sci. Technol.* **2003**, *63*, 1203.
(11) Gonella, F.; Cattaruzza, E.; Battaglin, G.; D'Acapito, F.; Sada, C.; Mazzoldi, P.; Maurizio, C.; Mattei, G.; Martorana, A.; Longo, A.; Zontone, F. *J. Non-Cryst. Solids* **2001**, *241*, 280.

(12) Rapallo, A.; Rossi, G.; Ferrando, R.; Fortunelli, A.; Curley, B. C.; Lloyd, L. D.; Tarbuck, G. M.; Johnston, R. L. *J. Chem. Phys.* **2005**, *122*, 194308.

(13) Chen, F.; Johnston, R. L. *Acta Mater.* **2008**, *56*, 2374.

(14) Ferrando, R.; Jellinek, J.; Johnston, R. L. *Chem. Rev.* **2008**, *108*, 845.

(15) Hillyard, S.; Silcox, J. *Ultramicroscopy* **1995**, *58*, 6.

(16) Aden, A. L.; Kerker, M. *J. Appl. Phys.* **1951**, *22*, 1242.

(17) Johnson, P. B.; Christy, R. W. *Phys. Rev. B* **1972**, *6*, 4370.

(18) Hövel, H.; Fritz, S.; Hilger, A.; Kreibig, U. *Phys. Rev. B* **1993**, *48*, 18178.

(19) de Ruijter, W. J.; Sharma, R.; McCartney, M. R.; Smith, D. J. *Ultramicroscopy* **1995**, *57*, 409.

(20) Battaglin, G.; Catalano, M.; Cattaruzza, E.; D'Acapito, F.; De Julian Fernandez, C.; De Marchi, G.; Gonella, F.; Mattei, G.; Maurizio, C.; Mazzoldi, P.; Miotello, A.; Sada, C. *Nucl. Instrum. Methods Phys. Res., Sect. B* **2001**, *178*, 176.

(21) Collins, D. R.; Schroder, D. K.; Sah, C. T. *Appl. Phys. Lett.* **1962**, *8*, 323.

(22) Miotello, A.; De Marchi, G.; Mattei, G.; Mazzoldi, P.; Sada, C. *Phys. Rev. B* **2001**, *63*, 075409.

JP809178Y